Quasiparticle bands and optical spectra of highly ionic crystals: AlN and NaCl

F. Bechstedt, K. Seino, P. H. Hahn, and W. G. Schmidt*
Institut für Festkörpertheorie und -optik, Friedrich-Schiller-Universität, Max-Wien-Platz 1, 07743 Jena, Germany
(Received 12 August 2005; revised manuscript received 27 October 2005; published 21 December 2005)

Based on the *ab initio* density functional theory we study the influence of many-body effects on the quasiparticle (QP) band structures and optical absorption spectra of highly ionic crystals. Quasiparticle shifts and electron-hole interaction are studied within the GW approximation. In addition to the electronic screening the effect of the lattice polarizability is discussed in detail. Substantial effects are observed for QP bands of AlN and NaCl that have large polaron constants of 1–2. The effect of electronic and lattice polarization on the optical spectra is discussed in terms of dynamical screening and vertex corrections. The results are critically discussed in the light of experimental data available. We find that measured peak positions can be reproduced without lattice polarizability in the screening of the electron-hole interaction and a reduced lattice contribution to the QP shifts.

DOI: 10.1103/PhysRevB.72.245114 PACS number(s): 71.20.−b, 71.15.Qe

I. INTRODUCTION

Single-particle and two-particle electronic excitations are accompanied by the rearrangement of the remaining electrons in a solid. This effect is known as screening of excited electrons (above the Fermi level) and excited holes (missing electrons below the Fermi level). The calculation of such electronic excitations has made substantial progress in the last decades, in particular using the framework of the many-body perturbation theory (MPBT).[1] In the case of clusters and molecular structures also the density-functional response theory is applied.[2] The most common assumption in the MBPT is the GW approximation (GWA) of Hedin[3,4] which describes the response of the electrons by a dynamically screened Coulomb potential W. In this approximation the self-energy operator Σ of an excited particle is given as a product of the potential W and the Green's function G. The poles of the G function correspond to the energies of the dressed particles, the quasiparticles. Electron-hole pair excitations are described by a special two-particle Green's function, the so-called (irreducible) polarization function P. It obeys a Bethe-Salpeter equation (BSE).[5,6] Apart from an electron-hole exchange (local-field effect) term proportional to the bare Coulomb potential v, its kernel is dominated by the variational derivative $\delta\Sigma/\delta G$ and hence by the screened potential W in random-phase approximation (RPA) which is already used in GWA and describes the attractive interaction of quasielectrons and quasiholes.[7]

The quasiparticle (QP) band structures of semiconductors and insulators are now well described by means of *ab initio* methods based on the density-functional theory[8] (DFT) within the local-density approximation (LDA) for exchange and correlation (XC).[9] For DFT-LDA bands with a correct energetical order the QP effects can be included by means first-order perturbation theory with respect to the difference of the XC self-energy and the XC potential already used in the Kohn-Sham equation of the DFT. Its numerical implementation[10,11] usually yields single-particle excitation energies in good agreement (with an accuracy of about 0.1 eV) with angle-resolved photoemission/inverse photoemission experiments.[12–14] Solutions of the BSE in an *ab initio* framework also appeared in the literature in the past few years. Optical spectra can now be calculated including excitonic effects for semiconductors and insulators,[15–17] solid surfaces,[18,19] and even molecules.[17,20,21] These effects can also be included in nonlinear optical properties.[22] All these calculations are based on computations of the dielectric matrix within the independent-particle approximation or a model dielectric function for the electronic system. The same calculational scheme has been also applied to wide-gap insulators, such as LiF and MgO,[23,24] and wide gap semiconductors, e.g., AlN.[25] These materials possess a remarkable ionic contribution to the total chemical bonding. The bond ionicity on an *ab initio* scale is given by the charge asymmetry coefficient g with values $g=0.794$ (AlN) and $g=0.958$ (NaCl).[26]

Polar materials are characterized by longitudinal-optical (LO) phonons whose excitation induces large macroscopic electric fields in the crystal.[27] These fields strongly couple to the excited electrons and holes and modify their motion. Therefore, the question arises whether or not the lattice polarizability contributes to the dressing of the quasiparticles and the screening of the electron-hole attraction. Ionic crystals with big dynamical ion charges should show strong lattice polaron effects modifying the electronic states near the band edges.[28] Such systems have small static dielectric constants ε_0 and ε_∞ and relatively large longitudinal optical phonon frequencies ω_{LO}. Because the static lattice polarizability $(\varepsilon_0-\varepsilon_\infty)$ is of the same order of magnitude as the static electronic dielectric polarizability $(\varepsilon_\infty-1)$ at high frequencies $\omega \gg \omega_{LO}$, large polaron constants $\alpha_p=(1/\varepsilon_\infty-1/\varepsilon_0)\times(\hbar/2ma_B^2\omega_{LO})^{1/2}$ (a_B-Bohr radius) result,[28] for instance $\alpha_p \approx 1.2$ or ≈ 2.0 for binary systems such as AlN and NaCl, respectively. They yield non-negligible polaron shifts $\mp\alpha_p\hbar\omega_{LO}$ of about 0.1–0.4 eV if perturbation theory can be applied to electron or hole states. However, it is not clear (i) how the lattice polarization really influences the quasiparticle bands and (ii) whether or not the lattice polarization plays a role on the time scale of the formation of a Coulomb-correlated electron-hole pair. There are several open questions concerning the theoretical description of excitations in

systems with high lattice polarizability. For instance, the peak positions in the optical absorption of wurtzite AlN with respect to experimental findings[25] are underestimated, and the position of the bound electron-hole-pair peak in the optical absorption and the exciton binding in NaCl[29] are not clear.

In this work, we study the quasiparticle band structures and optical spectra of NaCl and AlN. The calculations are based on the screening reaction of the strongly inhomogeneous electron gases. In addition, we show how the lattice polarizability $\sim(\varepsilon_0-\varepsilon_\infty)$ modifies the results for the single-particle excitation energies and the dielectric function in the framework of the GWA. We proceed in three steps: (i) We use the density functional theory in local density approximation to obtain the structurally relaxed ground state configurations of the ionic crystals, wurtzite (*w*-) and zinc-blende (*zb*-)AlN and rocksalt (*rs*-)NaCl, and the Kohn-Sham (KS) eigenvalues and eigenfunctions that enter the computation of the single- and two-particle Green's functions. (ii) The electronic quasiparticle spectrum is obtained within the GW approximation to the exchange-correlation self-energy with a dielectric tensor modified by the lattice polarization, and (iii) the Bethe-Salpeter equation is solved for coupled electron-hole pair excitations, thereby accounting for the screened electron-hole attraction and the unscreened electron-hole exchange. The paper is organized as follows. In Sec. II, we briefly summarize the basic theory formulation. In Sec. III, we present the quasiparticle band structure results with and without lattice polarization. In Sec. IV, our results for the optical absorption and electron-energy loss spectra are given. We discuss where lattice polarization may play a role. Finally, a short summary is given in Sec. V.

II. BASIC THEORETICAL FORMULATION

A. Ground state

Most of the ground-state properties of the crystals under consideration here have been obtained within density-functional theory[8] and local density approximation[9] as implemented in the VASP code.[30] The Perdew-Zunger interpolation[31] has been used for the XC energy in LDA. The interaction of the valence electrons with the nuclei is modeled by means of pseudopotentials (PPs) in accordance with the projector-augmented wave (PAW) method[32] which are rather similar to the ultrasoft pseudopotentials.[33] For AlN we have used softer and harder PPs. To achieve convergence cutoff energies of 17 or 26 Ry have been checked. In the case of NaCl this value has been tested to be 18 Ry. In addition, we present results for NaCl that have been obtained with a massively parallelized multigrid implementation of the DFT-LDA.[34] In this case *first-principles* normconserving PPs have been generated within the Hamann scheme.[35] Nonlinear core corrections,[36] which are particularly important for sodium, have also been taken into account.

The structural parameters calculated for *w*-AlN are listed in Table I. They are in reasonable agreement with experimental data[37] and results of other calculations (see, e.g., Ref. 38). The underestimated theoretical *a*-lattice constant is a consequence of the overbinding effect of the LDA for the given exchange-correlation energy. This effect with an almost 1% reduction of the theoretical lattice constant with respect to the experimental one is also observed for *zb*-AlN with $a_0=4.323$ Å (compared to $a_0=4.38$ Å from experiment[39]). For *rs*-NaCl we derived a theoretical cubic lattice constant of $a_0=5.435$ Å from the minimization of the total energy. It is again smaller than the experimental lattice constant of $a_0=5.64$ Å[40] but the deviations are larger than that in the AlN case. Nevertheless we calculated the electronic and optical properties at the theoretical lattice constants. For NaCl we have repeated the calculations done with the real-space code[34] by using VASP.[30] However, we did not found significant differences. Especially the Kohn-Sham eigenvalues agreed well.

TABLE I. Structural parameters of *w*-AlN. They are the lateral lattice constant a (in Å), the ratio c/a of the two lattice constants, and the internal-cell parameter u. The values calculated with soft and hard pseudopotentials are compared with results of a previous calculation (Ref. 38) and experimental data (Ref. 37.)

Parameter	Soft PP	Hard PP	Previous (Ref. 38)	Experiment (Ref. 37)
a	3.07	3.08	3.08	3.11
c/a	1.607	1.604	1.607	1.601
u	0.3815	0.3817	0.3824	0.3821

B. Quasiparticle bands

In order to account for the excitations aspect we replace the local XC potential $V^{XC}(\mathbf{x})$ in the Kohn-Sham equation of the ground state by a nonlocal and energy-dependent self-energy operator $\Sigma(\mathbf{x},\mathbf{x}';\varepsilon)$ and obtain the quasiparticle equation.[10–14] For the XC self-energy we apply the GW approximation,[3,4]

$$\Sigma(\mathbf{x},\mathbf{x}';\varepsilon)=\frac{i\hbar}{2\pi}\int d\omega e^{-i\omega 0^+}G(\mathbf{x},\mathbf{x}';\varepsilon-\hbar\omega)W(\mathbf{x},\mathbf{x}';\omega). \tag{1}$$

In practical evaluations, the one-particle Green's function G is described approximately in terms of the results of the DFT-LDA band structure calculation. The new QP bands $\varepsilon_n^{QP}(\mathbf{k})$ are obtained from the Kohn-Sham eigenvalues $\varepsilon_n(\mathbf{k})$ shifted by diagonal matrix elements of the difference between the self-energy and the XC potential calculated with Kohn-Sham eigenfunctions $\psi_{n\mathbf{k}}(\mathbf{x})$ by[10,41]

$$\varepsilon_n^{QP}(\mathbf{k})=\varepsilon_n(\mathbf{k})+\frac{1}{1+\beta_{n\mathbf{k}}}\{\Sigma_{n\mathbf{k}}^{\mathrm{COH}}+\Sigma_{n\mathbf{k}}^{\mathrm{SEX}}+\Sigma_{n\mathbf{k}}^{\mathrm{dyn}}[\varepsilon_n(\mathbf{k})]-V_{n\mathbf{k}}^{\mathrm{XC}}\}, \tag{2}$$

where the self-energy operator Σ has been divided into two static contributions, the Coulomb hole (COH) part and the screened exchange (SEX) part,[4] as well as a dynamic (dyn) contribution. Thereby, $\beta_{n\mathbf{k}}$ is the linear coefficient in the Taylor expansion of Σ^{dyn} around the KS eigenvalue $\varepsilon_n(\mathbf{k})$.

The major bottleneck in the GW calculations is the computation of the screened interaction W and the inverse dielec-

tric function ε^{-1}, respectively. An extreme acceleration can be achieved by using a model dielectric function for the response of the inhomogeneous electron gas in the presence of excited electrons and/or holes. Several functional forms have been suggested.[42,43] For systems with not too large gaps an accuracy of the band energies with respect to the valence-band maximum (VBM) of the order of 0.1 eV has been achieved.[44,45] We use the version suggested by Bechstedt *et al.*[41] It allows for analytic solutions for the dynamic contribution and the COH term. For instance, the static Coulomb hole contribution to the self-energy takes the form of a local potential. For cubic systems it holds

$$\Sigma^{\mathrm{COH}}(\mathbf{x},\mathbf{x}') = -\frac{q_{TF}(\mathbf{x})}{2}\sqrt{1-\frac{1}{\varepsilon_\infty}}\left[1+\frac{q_{TF}(\mathbf{x})}{k_F(\mathbf{x})}\times\sqrt{\frac{3\varepsilon_\infty}{\varepsilon_\infty-1}}\right]^{-1/2}\delta(\mathbf{x}-\mathbf{x}'), \tag{3}$$

where the Fermi (k_F) and Thomas-Fermi (q_{TF}) wave vectors, respectively, are computed at the local electron density $n(\mathbf{x})$. Local-field effects on the screening in the SEX contribution are approximated by using state-averaged electron densities. All occurring matrix elements are performed with Kohn-Sham eigenfunctions independent of the used multigrid representation[45] or the PAW representation.[46]

A more extended description of the details of the application of a model dielectric function and the approximate treatment of the local-field and dynamical screening effects has been published in Refs. 41, 43, and 46. The most important numerical advantage is that the sum over intermediate states in Σ^{dyn} can be analytically carried out. No explicit dependence on the number of conduction bands occurs in the computation of this self-energy operator. The results for Si, GaAs, AlAs, and ZnSe show agreement with the full GW calculations to within 0.2 eV for all the states considered. Successful applications were also made to wide-gap semiconductors such as GaN,[47] SiC,[48] and BN.[49] Similar to the standard GW treatment of the quasiparticle band structure, also the scheme based on a model dielectric function neglects self-consistency effects and vertex corrections.[13,14]

C. Pair excitations and optical spectra

Excitation energies obtained within the quasiparticle formalism describe one-particle excitations, such as those involved in direct or inverse photoemission experiments. For the description of the optical properties, however, one needs to go beyond the single-particle level. We study the diagonal elements of the macroscopic dielectric function $\varepsilon_{jj}(\omega)$. They are related to the polarization function P of the electronic system. Using a representation in Kohn-Sham eigenfunctions one has in the limit of vanishing photon wave vectors[7,50]

$$\varepsilon_{jj}(\omega) = 1 - \frac{8\pi e^2\hbar^2}{V}\sum_{c,v,\mathbf{k}}\sum_{c',v',\mathbf{k}'}\{M^j_{cv}(\mathbf{k})M^{j^*}_{c'v'}(\mathbf{k}') \times P(cv\mathbf{k},c'v'\mathbf{k}';\omega) + \text{c.c. and } \omega\leftrightarrow-\omega\} \tag{4}$$

with matrix elements of the velocity operator $\mathbf{v}$

$$M^j_{cv}(\mathbf{k}) = \frac{\langle c\mathbf{k}|v_j|v\mathbf{k}\rangle}{\varepsilon_c(\mathbf{k})-\varepsilon_v(\mathbf{k})} \tag{5}$$

and V the normalization volume. In (4) the sums run over pairs of electrons in empty conduction band states $|c\mathbf{k}\rangle$ and holes in occupied valence band states $|v\mathbf{k}\rangle$, which are virtually or physically excited by photons of energy $\hbar\omega$.

The polarization function P obeys a BSE. However, one has to introduce additional approximations to derive a closed equation for the polarization function $P(cv\mathbf{k},c'v'\mathbf{k}';\omega)$ that depends only on one frequency. The contribution to the kernel of the screened potential with respect to the single-particle Green's function has to be neglected.[51] Moreover, the screening of the Coulomb attraction of electron and hole is assumed to be static.[7] Neglecting the coupling of resonant and antiresonant electron-hole pairs as well as the non-particle-conserving contributions to the electron-hole interaction,[15] the polarization function obeys a BSE of the standard form

$$\sum_{c'',v'',\mathbf{k}''}\{H(cv\mathbf{k},c''v''\mathbf{k}'')-\hbar(\omega+i\gamma)\delta_{cc''}\delta_{vv''}\delta_{\mathbf{kk}''}\}\times P(c''v''\mathbf{k}'',c'v'\mathbf{k}';\omega) = -\delta_{cc'}\delta_{vv'}\delta_{\mathbf{kk}'} \tag{6}$$

with the effective electron-hole pair Hamiltonian $H(cv\mathbf{k},c'v'\mathbf{k}')$ and a small damping γ of the pair excitations. The Hamiltonian of pairs of excited electrons and holes, more precisely, of quasielectrons and quasiholes, is given by[5,6,15,50]

$$H(cv\mathbf{k},c'v'\mathbf{k}') = [\varepsilon^{QP}_c(\mathbf{k})-\varepsilon^{QP}_v(\mathbf{k})]\delta_{cc'}\delta_{vv'}\delta_{\mathbf{kk}'} + W(cv\mathbf{k},c'v'\mathbf{k}') + \bar{v}(cv\mathbf{k},c'v'\mathbf{k}') \tag{7}$$

with the matrix elements

$$W(cv\mathbf{k},c'v'\mathbf{k}') = -\int d^3\mathbf{x}\int d^3\mathbf{x}'\,\psi^*_{c\mathbf{k}}(\mathbf{x})\psi_{c'\mathbf{k}'}(\mathbf{x})\times W(\mathbf{x},\mathbf{x}')\psi_{v\mathbf{k}}(\mathbf{x}')\psi^*_{v'\mathbf{k}'}(\mathbf{x}') \tag{8}$$

and

$$\bar{v}(cv\mathbf{k},c'v'\mathbf{k}') = 2\int d^3\mathbf{x}\int d^3\mathbf{x}'\,\psi^*_{c\mathbf{k}}(\mathbf{x})\psi_{v\mathbf{k}}(\mathbf{x})\bar{v}(\mathbf{x}-\mathbf{x}')\times\psi_{c'\mathbf{k}'}(\mathbf{x}')\psi^*_{v'\mathbf{k}'}(\mathbf{x}') \tag{9}$$

of the (statically) screened Coulomb interaction $W(\mathbf{x},\mathbf{x}')$ and a bare Coulomb interaction $\bar{v}(\mathbf{x}-\mathbf{x}')$. Only the short-range part of the latter is taken into account in agreement with the physical character of expression (9) as electron-hole exchange.[6] The matrix elements (5), (8), and (9) are again computed using the real-space representation[45,50] or within the PAW picture.[32,52] Usually the static screening in (8) is sufficient for reasonable spectral properties on the two-particle level.[53]

The eigenvalues and eigenvectors of the two-particle Hamiltonian (7) can be used to calculate directly the frequency-dependent dielectric function (4). Thereby we ap-

ply a typical broadening $\gamma=0.15$ or 0.20 eV of the electron-hole pairs. The rank of the Hamiltonian matrix (7) is governed by the number of valence (v) and conduction (c) bands and the number of **k** points in the Brillouin zone (BZ). In the case of the cubic crystals with an fcc Bravais lattice, we typically take four valence and four conduction bands into account. The BZ is sampled by 4000 random **k** points. They are generated by means of a random number generator. Special points such as of the Monkhorst-Pack type[54] may give rise to a faster convergence in the calculations of the interband density of states. However, random **k** points distributed over the entire BZ give rise to a faster convergence after inclusion of the strong electron-hole interaction. This has been recently demonstrated for silicon.[55] The resulting number of 48000 pair states is nearly conserved in the wurtzite case by doubling the number of bands but reducing the number of points in the BZ. Such an approach requires the diagonalization of large-rank matrices. In order to bypass the diagonalization of the Hamiltonian (7), we have developed a numerically more efficient initial-state method[19,50] to calculate the optical polarizability, which is essentially the product of the transition matrix elements (5) and the polarization function (6). This quantity obeys an evolution equation driven by the Hamiltonian (7). In the case of *w*-AlN we double the number of bands but restrict the BZ sampling to 1000 random **k** points. For NaCl the bands are more flat comparing with AlN. For that reason we slightly reduce the BZ sampling to 300 random **k** points when using a conventional unit cell with 8 atoms.

D. Lattice polarizability

Usually the screened interaction W in Secs. II B and II C only contains the response of the inhomogeneous electron gas. For strongly ionic systems with large lattice polarizabilities the question arises how the motion of the nuclei will effect the energies and strengths of electronic single-particle and pair excitations. An answer may be given by taking the electron-phonon interaction into account. There are many papers that have been addressed to this problem (see Ref. 28 and references therein). On the other hand, the GW approximation suggests a simple way to study the influence of the lattice motion, in particular the motion of charged ions, by modifying the screening of the coupled electron-lattice system. The effect of the lattice polarizability may be described by a modified frequency-dependent dielectric matrix of the crystal

$$\varepsilon(\mathbf{q}+\mathbf{G},\mathbf{q}+\mathbf{G}';\omega)=\delta_{\mathbf{G}G'}+4\pi\alpha_{el}(\mathbf{q}+\mathbf{G},\mathbf{q}+\mathbf{G}';\omega)+4\pi\alpha_{lat}(\mathbf{q}+\mathbf{G},\mathbf{q}+\mathbf{G}';\omega) \qquad (10)$$

with

$$\alpha_{el}(\mathbf{q}+\mathbf{G},\mathbf{q}+\mathbf{G};0)=\frac{1}{4\pi}\frac{1}{\frac{1}{\varepsilon_\infty-1}+|\mathbf{q}+\mathbf{G}|^2/q_{TF}^2+|\mathbf{q}+\mathbf{G}|^4/\left(\frac{4}{3}k_F^2q_{TF}^2\right)}.$$

The most important electronic contribution α_{el} to the polarizability of the crystal is taken in a form described elsewhere.[41,46,50] In the strongly ionic crystals under consideration, in addition, there exists a contribution α_{lat} of the polarizable lattice. In the long-wave-length limit ($\mathbf{G}=\mathbf{G}'=0,\mathbf{q}\to 0$) it is given as[27,56]

$$\alpha_{lat}(\mathbf{q}\to 0,\mathbf{q}\to 0;\omega)=\frac{1}{4\pi}\sum_{\alpha=x,y,z}\hat{q}_\alpha^2[\varepsilon_{\alpha\alpha}(\omega)-\varepsilon_{\infty\alpha}],$$

$$\varepsilon_{\alpha\alpha}(\omega)=\varepsilon_{\infty\alpha}\left[1+\frac{\omega_{LO}^2(\alpha)-\omega_{TO}^2(\alpha)}{\omega_{TO}^2(\alpha)-(\omega+i0^+)^2}\right] \qquad (11)$$

with $\hat{\mathbf{q}}=\mathbf{q}/|\mathbf{q}|$, the zone-center optical frequencies $\omega_{LO}(\alpha)$ and $\omega_{TO}(\alpha)$, and $\varepsilon_{0\alpha}=\varepsilon_{\alpha\alpha}(0)$ or $\varepsilon_{\infty\alpha}=\varepsilon_{\alpha\alpha}(\omega\gg\omega_{LO}(\alpha))$. In the case of the uniaxial wurtzite crystals with four atoms in the unit cell, expression (11) is generalized to a direction-dependent quantity because of the two independent tensor components $\varepsilon_{xx}(\omega)=\varepsilon_{yy}(\omega)$ and $\varepsilon_{zz}(\omega)$. In this case the phonon frequencies have to be replaced by those of $E_1(A_1)$ symmetry for the $xx=yy(zz)$ component.

The quantities $\varepsilon_{\infty\alpha}$ in expression (11) represent the static electronic dielectric constants of the semiconductor or insulator under consideration. The total static dielectric constants $\varepsilon_{0\alpha}$ of the polar crystal are enlarged by the static lattice polarizability. In a hexagonal or cubic crystal the dielectric constants obey the Lyddane-Sachs-Teller relation $\varepsilon_{0\alpha}/\varepsilon_{\infty\alpha}=[\omega_{LO}(\alpha)/\omega_{TO}(\alpha)]$.[2,27,56] The tensor character of the dielectric constants in the wurtzite case has been neglected in the many-body calculations. In the literature there is a body of varying dielectric constants. In the many-body calculations we use reliable values $\varepsilon_\infty=4.4$ and $\varepsilon_0=9.14$ for both *w*- and *zb*-AlN.[38,57] For *rs*-NaCl these values are $\varepsilon_\infty=2.35$ and $\varepsilon_0=5.45$.[58] In the case of AlN the used values are close to such derived from RPA or density-functional perturbation theory calculations.[38,57]

E. Inclusion of lattice polarizability

The replacement of the dielectric matrix by expression (10) has a great advantage. The response of both electron gas and ionic lattice can be described simultaneously for any electronic excitation, electron, hole, and electron-hole pair. In the limit of small wave vectors and frequencies, $\alpha_{el}(\mathbf{q}+\mathbf{G},\mathbf{q}+\mathbf{G}';\omega)=(1/4\pi)(\varepsilon_\infty-1)\delta_{\mathbf{GG}'}$, the imaginary part of the inverse matrix reads as ($\omega>0$)

$$\mathrm{Im}\,\varepsilon^{-1}(\mathbf{q}+\mathbf{G},\mathbf{q}+\mathbf{G}';\omega)=\frac{\pi}{2}\frac{\omega_{LO}^2-\omega_{TO}^2}{\omega_{LO}\varepsilon_\infty}\delta(\omega_{LO}-\omega)\delta_{\mathbf{GG}'}=\frac{\pi}{2}\left(\frac{1}{\varepsilon_\infty}-\frac{1}{\varepsilon_0}\right)\omega_{LO}\delta(\omega_{LO}-\omega)\delta_{\mathbf{GG}'}. \qquad (12)$$

The prefactor in (12), $\sim(1/\varepsilon_\infty-1/\varepsilon_0)$, dominates the Fröhlich coupling constant of the interaction between electrons and longitudinal optical phonons (Ref. 28 and references therein). The expression (12) immediately yields the self-energy of an electron or hole polaron using the spectral representation of the self-energy (1).[28] The discussed small

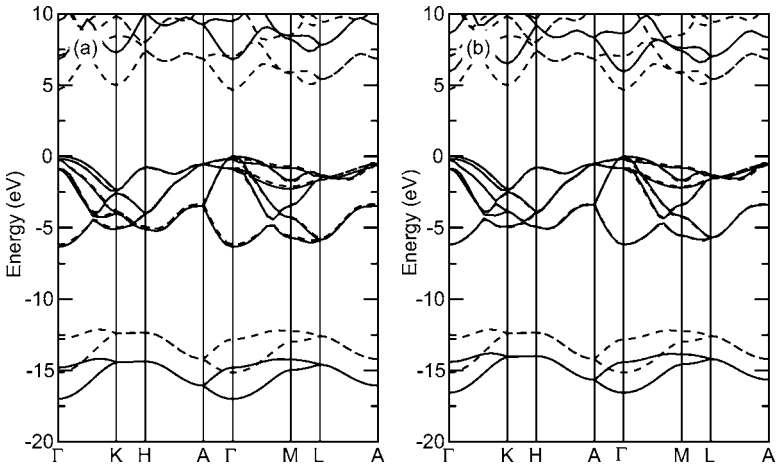

FIG. 1. Quasiparticle bands (solid lines) without (a) and with (b) the effect of the lattice polarization in comparison with Kohn-Sham bands (dashed lines) for *w*-AlN. The valence-band maximum is used as energy zero. Soft pseudopotentials have been used.

wave-vector and frequency limit is also relevant for weakly bonded electron-hole pairs, the Wannier-Mott excitons.[28] Because of their characteristic large radii the electron-hole exchange contributions (9) are negligible. The small binding energies allow that the lattice can completely follow the exciton formation, and the attractive Coulomb interaction (8) has to be screened by the static dielectric constant ε_0 which includes the static lattice polarizability besides the electronic effect.[59–61]

For negligible static lattice polarization $(\varepsilon_0-\varepsilon_\infty)\to 0$ also the dynamic lattice polarizability (11) vanishes. Then both the quasiparticle effects in (2) as well as the electron-hole attraction (8) are dominated by the pure electronic screening. Corrections due to the vibrating lattice may be derived in a straightforward manner. For small lattice polarizabilities one obtains the result of Hedin and Lundqvist[4] for the influence of the vibrating lattice on the screened potential W. In a formal description the polarizability in (10) can be replaced according to $4\pi\alpha=vP$ by the bare Coulomb potential v and the polarization function P of the system. Taking electronic and lattice polarization into account according to (10), one finds formally for the screened interaction

$$W = v[1 - v(P_{el} + P_{lat})]^{-1}. \tag{13}$$

A Taylor expansion yields in first order to

$$W = W_{el} + W_{el}P_{lat}W_{el} \tag{14}$$

with $W_{el}=v[1-vP_{el}]^{-1}$. Expression (14) has been used by Hedin and Lundqvist[4] to derive analytic formulas for the influence of phonons on the electron self-energy.

The application of the dielectric tensor (10) to describe the screening in the XC self-energy and in the BSE requires a careful discussion of the contributing characteristic wave vectors and frequencies and, consequently, then allows us appropriate approximations. The limit of complete neglect of lattice polarizability is the original approximation I. The full lattice polarization (11) acts only substantially in the long-wavelength limit. This is more or less automatically adjusted by formula (10). For wave vectors $|\mathbf{q}+\mathbf{G}|>q_{TF}$ the electronic screening dominates. For that reason, we will use the static limit of (10) as one possible approach labeled by approximation II. Practically only the static lattice polarizability $(\varepsilon_0-\varepsilon_\infty)$ is added to the (electronic) dielectric function (10) in the statically screened quantities Σ^{COH} (2), Σ^{SEX} (2), and W (8). The inclusion in the quasiparticle calculations is obvious. The dynamics in the self-energy is still dominated by the electronic response, since the QP shifts in (2) with respect to the KS eigenvales are large compared to the phonon frequencies. We will also introduce an approximation III where the lattice polarizability is only partially taken in the computation of the self-energy. In the explicit calculations we replace the dielectric constant by the average of the two values ε_∞ and ε_0.

The dynamics of screening influences very much the attractive electron-hole interaction. With the inclusion of the frequency dependence of the dielectric matrix in W (8) no closed BSE (6) can be derived for the two-particle polarization function depending only on one frequency.[7,53,59,60] For that reason we simulate effects of dynamical screening by studying the static screening for the two limiting cases. The strength of the screening, in particular in the BSE (6), depends sensitively on the strength of the Coulomb effects, in particular the exciton binding energy itself. In the case of the Wannier-Mott excitons the binding energies E_B are usually so small that $E_B<\hbar\omega_{LO}$ holds. Dynamical screening does not play a role. The complete static lattice polarizability $\sim(\varepsilon_0-\varepsilon_\infty)$ contributes to the screening of the electron-hole attraction.[59–61] The screening is mainly characterized by the static dielectric constant ε_0. In the opposite limit, $E_B>\hbar\omega_{LO}$, the lattice cannot follow the formation of bound electron-hole pairs and the Coulomb attraction is only screened by the redistribution of electrons. The electronic bands of NaCl are rather flat and the dielectric constant ε_∞ is small. One expects that the conditions for the second approximation are clearly fulfilled. AlN seems to represent an intermediate case. For that reason we investigate both situations, neglect of lattice polarizability in (8), i.e., use of ε_∞, and inclusion of lattice polarizability, i.e., use of ε_0 or an averaged value in the model dielectric function described in Refs. 41 and 43.

III. QUASIPARTICLE BAND STRUCTURES

The lattice effect on the quasiparticle excitations is illustrated in Fig. 1. It shows the QP band structures of *w*-AlN

TABLE II. Gaps E_g and valence-band widths E_w of *w*-AlN with and without lattice polarization. Soft pseudopotentials have been used. All values in eV.

	Present calc.			Previous calc. (Ref. 62)		Expt.	
Energy	KS	QP (without)	QP (with)	KS	QP (without)	(Ref. 63)	(Ref. 64)
E_g ($\Gamma-\Gamma$)	4.67	6.80	5.95	3.9	5.8	6.11	6.25
E_g ($\Gamma-K$)	5.00	7.28	6.51	4.8	6.7		
E_w (upper)	6.18	6.33	6.17	7.4	8.0		
E_w (total)	15.15	17.00	16.57	16.3	18.2		

using averaged dielectric constants $\varepsilon_\infty=4.4$ and $\varepsilon_0=9.14$ with and without lattice polarization in comparison to the KS bands. The positive (negative) QP shifts of the conduction (valence) bands are somewhat reduced in the presence of the lattice polarization. This observation is in agreement with the fact that lattice polaron effects shrink the gaps and transition energies.[28] The effect of the lattice polarizability scales with the QP effects themselves. Therefore, it mainly occurs in the *sp*-conduction bands and in the deep N2*s* valence bands. However, the reduction of the quasiparticle shifts by the lattice polarizability is stronger in the case of the empty states.

Explicit numbers are given in Table II for *w*-AlN and in Table III for *zb*-AlN. They show an opening of the gaps and transition energies by pure electronic QP shifts of 2.1–2.5 eV. The full inclusion of the lattice polarizability reduces these QP shifts. The lattice-polaron effect shrinks the quasiparticle fundamental gaps by about 0.6–0.9 eV. The comparison with direct gaps (*w*-AlN) and indirect gaps (*zb* -AlN) derived from measurements remains somewhat inclusive. Moreover, the experimental gap values show a considerable dependence on temperature.[66] In both the wurtzite and zinc-blende cases the QP gaps with and without lattice polarizability frame the experimental values. However, one has to take into consideration that gaps have generally been derived from optical measurements[63–65] (see also body of data in Ref. 67). Even in the case that excitonic effects have been separated, the extracted data may be influenced by vertex corrections of the gap due to the electron-phonon interaction. According to Mahan[28] the polaron shrinkage of the optical pair energies is governed by the difference $(g_e-g_h)^2$ of the coupling constants for electrons (g_e) and holes (g_h). In our GW quasiparticle calculations we take only the effect on electrons ($\sim g_e^2$) and holes ($\sim g_h^2$) into account. The vertex corrections $\sim -2g_eg_h$ do not occur. Consequently, the QP gaps calculated with the full inclusion of the lattice polarizability should be smaller than the gaps extracted from optical data. Because of the partial cancellation of the electron and hole effects due to $(g_e-g_h)^2$, one should expect QP gaps in between the values of Tables II and III computed with and without lattice polarizability.

There is another problem in the calculations. Our pure electronic QP openings are larger than the values obtained in a previous calculation[62] by 0.2 eV. One reason for this discrepancy may be due to the use of a larger dielectric constant $\varepsilon_\infty=4.84$.[62] More substantial are, however, the discrepancies in the DFT-LDA gaps of *w*-AlN. We find 4.67 eV instead of 3.9 eV.[62] This cannot only be explained by the use of different lattice constants, theoretical one (here) and experimental one in Ref. 62. To solve the discrepancy we repeated the DFT-LDA calculations with harder pseudopotentials but found only a small reduction of the gap value to 4.53 eV [see also Fig. 2(b)]. The majority of the previously calculated DFT-LDA gaps (Ref. 38; see also collection in Ref. 68) are close to our value. Within the generalized gradient approximation (GGA) of the XC potential in the KS equation, a gap of 4.74 eV has been computed. Our test calculations within the GGA framework[69] gave almost the same DFT band structures [see Fig. 2(a)]. Only the *s*-like conduction band minima are shifted towards smaller energies by about 0.1 eV. The indirect Kohn-Sham gap for *zb*-AlN is 3.33 eV (Table III). This value is also close to that of other DFT-LDA calculations of 3.1 eV.[70]

The effect of the lattice polarizability on other details of the band structure is much weaker. Interestingly the lattice polaron effect tends to narrow also the band widths of the valence bands (see Table II). Unfortunately the currently available measurements of the density of states[70] (DOS) do not give values for the valence-bands widths with a sufficient precision. Nevertheless, they indicate two interesting facts:

TABLE III. Fundamental gaps E_g (in eV) for *zb*-AlN with and without lattice polarizability. Soft pseudopotentials have been used.

	Present calc.			Previous calc. (Ref. 62)		Expt.
Gap	KS	QP (without)	QP (with)	KS	QP (without)	(Ref. 65)
$\Gamma\rightarrow\Gamma$	4.61	6.72	5.86	4.2	6.0	
$\Gamma\rightarrow X$	3.33	5.45	4.74	3.2	4.9	5.34
$\Gamma\rightarrow K$	5.20	7.67	6.78			
$\Gamma\rightarrow L$	7.66	10.15	9.25	7.3	9.3	

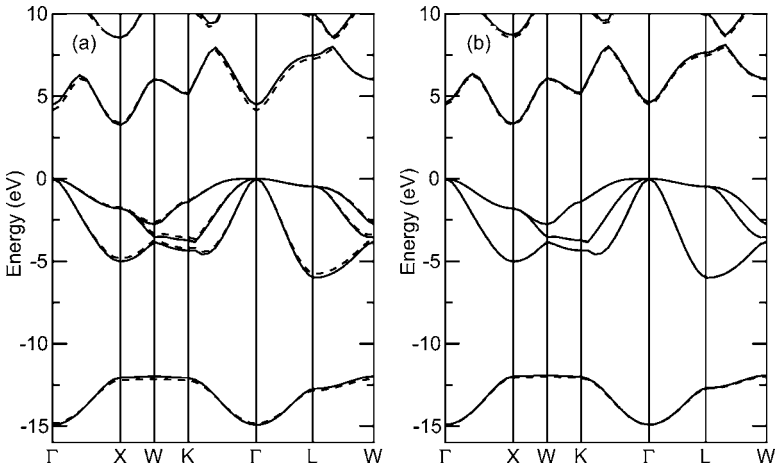

FIG. 2. Comparison of the Kohn-Sham bands (a) in LDA (solid lines) and GGA (dashed lines) or (b) using soft (solid lines) and hard (dashed lines) pseudopotentials for *zb*-AlN.

(i) The DOS of *zb*-AlN and *w*-AlN roughly agree in the valence-band region and (ii) the peak maximum in the DOS of the lowest valence bands is shifted to lower energies with respect to the DOS derived from the DFT-LDA. This value is in rough agreement with the QP shift (at least for the use of ε_0) as demonstrated in Fig. 1 and the increase of the valence-band width in Table II. There is also a small influence of the QP effects on the crystal-field splitting. Its absolute value is reduced from −205 meV (KS) to −190 meV (QP, without) and −182 meV (QP, with lattice polarizability). The recommended experimental value amounts to −169 meV.[67]

Quasiparticle energies for *rs*-NaCl are listed in Table IV and plotted in Fig. 3. The band structures also show the positions of energy peaks measured for critical points in the BZ by means of angle- and energy-resolved distributions of photoelectrons from the (100) face of NaCl single crystals. The fundamental QP gaps given in Table IV are 8.63 eV(ε_∞) and 7.17 eV(ε_0). Again they frame the experimental value of 8.5 eV derived from ultraviolet photoemission data[72] or others of about 8.5 eV[73] or 8.0 eV[74] and seem to suggest only a small contribution of the lattice relaxation (however, see discussion in Sec. IV). For that reason, results for the average 3.9 of the two dielectric constants ε_0 and ε_∞ and, hence, only 50% of the lattice polarizability are also given in Table IV. The gap opening by pure electronic screening of 3.51 eV is strongly reduced by 1.48 eV due to the inclusion of the full lattice polarizability in the static parts of the self-energy (2).

TABLE IV. Quasiparticle shifts of the VBM and the CBM as well as level positions of *rs*-NaCl with inclusion of the lattice polarizability in different approximations. All values in eV. The VBM in KS eigenvalues is used as energy zero.

Inclusion of lattice polarizability	Level	KS eigenvalue	QP shift	QP eigenvalue
without	CBM	5.14	1.95	7.09
	VBM	0	−1.55	−1.55
with partial	CBM	5.14	0.92	6.06
	VBM	0	−1.56	−1.56
with	CBM	5.14	0.73	5.87
	VBM	0	−1.30	−1.30

The reason is mainly related to the variation of the SEX term. The variation of the COH terms only contributes with about 25% to the lattice-polaron gap shrinkage. We mention that a QP gap opening due to pure electronic polarization effects of about 3.7 eV has been already predicted many years ago by Carlsson[75] and Harrison.[76]

The comparison with experimental band positions[71] in Fig. 3 leads to a similar conclusion as the discussion of the fundamental gaps in Table IV. The quasiparticle bands obtained for the pure electronic screening [Fig. 3(a)] are closer to the points measured with respect to the VBM or the conduction-band minimum (CBM). This holds particularly for the bands X_{5c}, $X_{4'c}$, X_{3c}, X_{1c}, $X_{5'v}$, and $X_{4'v}$ at the X point. The band state Γ'_{25c} is too high in energy whereas the band Γ_{12c} is too low. However, the agreement with the QP bands including partially lattice polarizability [Fig. 3(b)] is much worse. Altogether, comparing with the PES data of Steinmann and Himpsel[71] it seems that the QP band structure with pure electronic screening better describes the experimental findings. The reason may be related to the used initial-state technique to determine the valence-band states with respect to the VBM and the final-state technique to determine the conduction-band states with respect to the CBM. Another reason may be related to the fact that different bands are involved in the underlying emission processes. According to the vertex corrections of the polaron effect discussed already for AlN here also a cancellation should occur. The cancellation effects may be supported by the fact that both the highest valence band and the lowest conduction band are mainly derived from chlorine states.[77] This fact is somewhat in contrast to the anion character of the lowest conduction band in the case of the other alkali halides.[76,78]

IV. OPTICAL SPECTRA: EXCITONIC EFFECTS

As a first example the frequency-dependent dielectric function of *zb*-AlN is shown in Fig. 4 using a broadening parameter γ=0.2 eV and 4000 random **k** points in the BZ. Left panels [Fig. 4(a)] show the real and imaginary parts of the dielectric function within the independent QP approach. That means, the Coulomb effects $\sim W$ and $\sim \bar{v}$ in the pair Hamiltonian (7) have been disregarded. QP results are presented for pure electronic screening and screening including

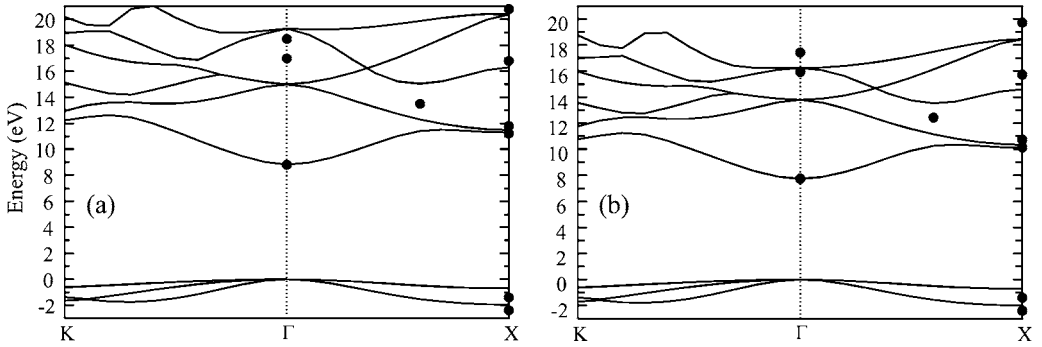

FIG. 3. Quasiparticle bands without (a) and with (b) the effect of the lattice polarization for *rs*-NaCl. The valence-band maximum is used as energy zero. The filled circles indicate measured band positions (Ref. 71).

the lattice polarizability. The right panels [Fig. 4(b)] give the same spectra with the inclusion of excitonic effects. The calculated curves are compared with measured spectra.[79] The QP spectra demonstrate that the most important effect of the inclusion of the lattice polarizability is an almost rigid redshift of about 0.8 eV. The lineshape is less influenced. On the other hand, the Coulomb correlations, screened electron-hole attraction and electron-hole exchange in (7), yield a drastic redistribution of the absorption spectrum (more strictly: imaginary part of the dielectric function). Spectral density is redistributed from the high-energy region closer to the region following the absorption onset in agreement with previous observations for other crystals.[50] This tendency is combined with an overall redshift of the absorption due to the Coulomb effects. However, no bound excitons are observed below the absorption onset within our numerical accuracy. Their reproduction may require denser **k**-point meshes. The redshift amounts to about 1.2 eV for the pure electronic screening and is reduced to 0.6 eV after inclusion of the lattice polarization. As a consequence of the different action of the lattice polarizability on the QP shifts and the Coulomb attraction, the optical spectra resulting for two different screenings, with and without lattice polarization, exhibit wide similarities. The spectrum with the larger screening is only less redshifted with respect to that computed for the pure electronic screening effect.

The question, which of the two computed spectra better fits to the measured one, is difficult to answer. The low-energy side of the absorption and the peak structure in the real part fit better to the neglect of the lattice polarizability. The reason may be the partial cancellation of the polaron effects due to vertex corrections (see discussion in Sec. III) and the dynamics of the screening in the electron-hole attraction. The spectral redshifts due to the excitonic effects are with 0.6 or 1.2 eV much larger than the optical phonon energies. As a consequence the spectrum computed with the pure electronic screening may be closer to the measured one. Conclusions within the Wannier-Mott exciton picture concerning the correct inclusion of dynamical screening are also very difficult. Using the band and dielectric parameters from Ref. 80 one finds different exciton binding energies of about 0.09 eV(ε_0) or 0.29 eV(ε_∞) in dependence of the dielectric constant. These values surround the optical phonon energy of 0.10 eV. This fact and the comparison of the theoretical and experimental spectra in Fig. 4(b) indicate that further studies are needed with an improved **k**-point sampling (on the theoretical side) and improved sample quality (on the experimental side).

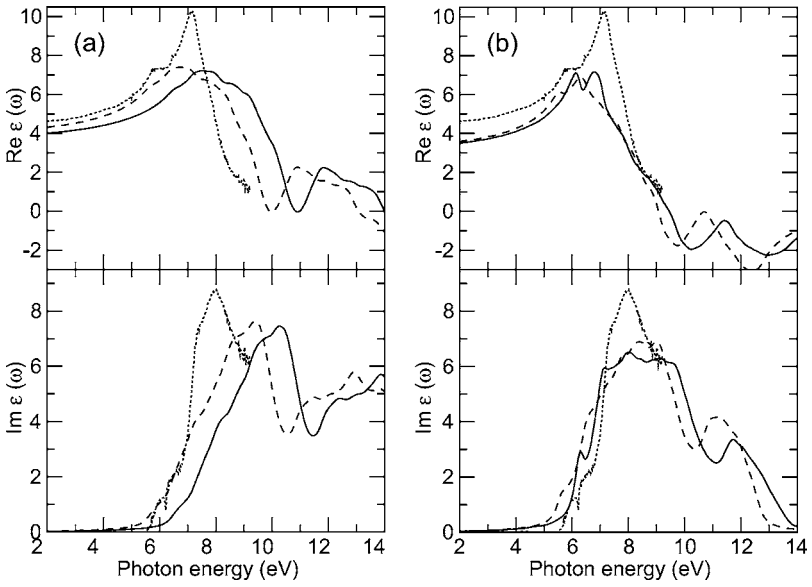

FIG. 4. Frequency-dependent macroscopic dielectric function of *zb*-AlN within the independent-quasiparticle approximation (a) and for Coulomb-correlated electron-hole pairs (b). The QP and excitonic effects have been calculated using pure-electronic screening (solid lines) or under inclusion of the lattice polarizability (dashed lines). The theoretical spectra are compared with experimental ones (dotted lines) (Ref. 79).

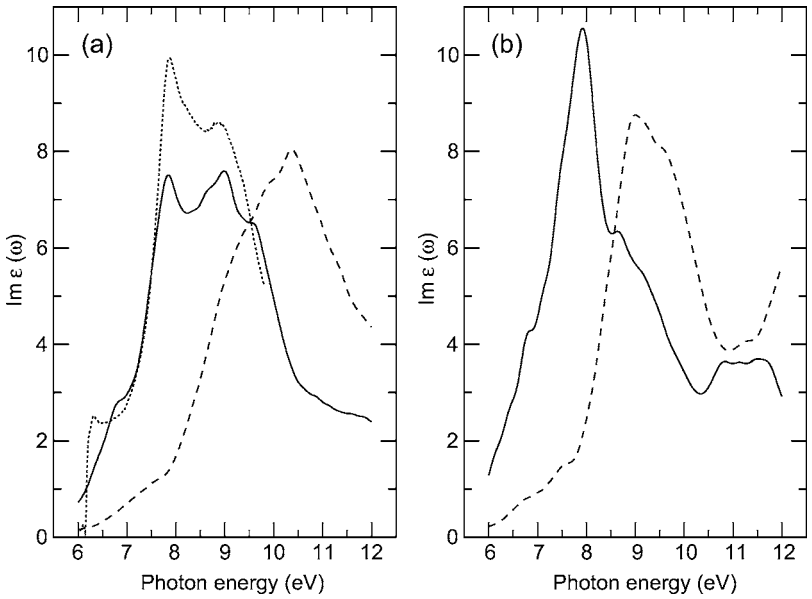

FIG. 5. Imaginary parts of the macroscopic dielectric function calculated including quasiparticle (dashed lines) and excitonic (solid lines) effects for *w*-AlN. The lattice polarization has been neglected. Ordinary (a) and extraordinary (b) light polarizations are studied. An experimental spectrum (Ref. 79) is shown as dotted line. A Lorentzian broadening of $\gamma=0.2$ eV and 1000 random **k** points in the BZ have been used.

The optical absorption spectra for ordinary and extraordinary light polarization are presented in Fig. 5 for *w*-AlN. This figure again demonstrates the huge excitonic effects in the AlN case. The spectra calculated within the framework of independent quasiparticles are completely redistributed from higher to lower photon energies. Thereby, the lineshape changes remarkably. The imaginary part of the ordinary dielectric function shows not only qualitative but also quantitative agreement with the measured spectrum. The positions of the two main peaks at 7.8 and 9.0 eV (computed spectrum) are in excellent agreement with the results of spectroscopic ellipsometry measurement.[79,81] Only the steep onset of the absorption is less pronounced in the calculated spectrum because of the use of random **k** points. They do not give rise to converged contributions from the lowest optical transitions from the Γ-point region to the joint density of states. The peak intensities are somewhat below the experimental values. However, in fact in a previous measurement[25] smaller intensities have been obtained. Because of the reproduction of the peak positions we have only used pure electronic screening in the spectra computation for Fig. 5. The partial inclusion of the lattice polarizability, at least in the determination of the QP band structure, would give a redshift of the theoretical absorption spectra in disagreement with the experimental findings.

The influence of the many-body effects according to (2) and (7) on the optical absorption of *rs*-NaCl is illustrated in Fig. 6. It presents spectra which account for both excitonic and quasiparticle effects or only for quasiparticle effects. For comparison the imaginary part of the dielectric function for independent Kohn-Sham particles is also shown. Only electronic screening effects have been taken into account. The spectra have been computed using the real-space approach.[34] A conventional simple cubic (sc) unit cell with 8 atoms has been used. The smaller sc BZ has been sampled with a reduced number of 300 random **k** points. Comparing the DFT-LDA and the QP spectra an overall characteristic blueshift of about 3.7 eV is visible. However, the lineshape remains almost conserved. The high-energy peaks are seemingly be related to optical transitions between band states in Fig. 3. However, the inclusion of the screened electron-hole attraction and the electron-hole exchange gives rise to a complete redistribution of the optical spectrum. A strong bound exciton peak occurs at the absorption edge while the spectrum for higher photon energies is remarkably reduced. Such tendencies have been also observed for another alkali halide, LiF.[24] However, in the case of NaCl it is difficult to derive an exciton binding energy directly from the comparison of the QP spectra with and without excitonic effects. The bound exciton peak whose broadening is dominated by the value $\gamma=0.2$ eV sits practically at the fundamental QP gap value. The reason is that not only the lowest interband transitions cv contribute to the exciton but also higher optical transitions $c'v'$ which are mixed in by the matrix elements of W (8) and $\bar{v}$ (9). Consequently, it makes no sense to ask directly for an

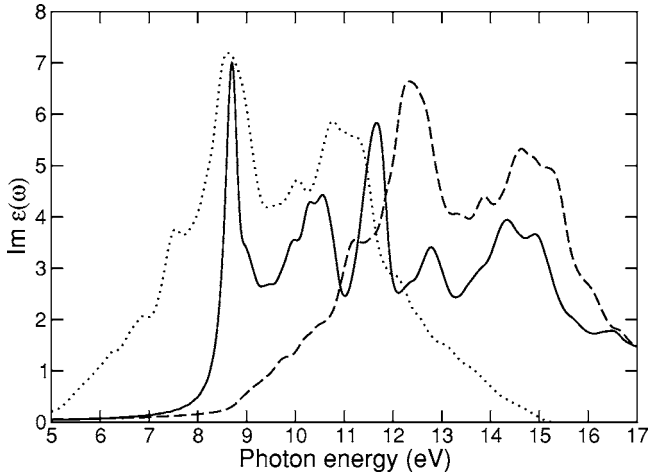

FIG. 6. Imaginary part of the dielectric function of *rs*-NaCl including quasiparticle and excitonic effects (solid line), within the independent quasiparticle approximation (dashed line), and the independent Kohn-Sham-particle approximation (dotted line). Only pure electronic screening has been taken into account. A broadening of $\gamma=0.2$ eV is used.

exciton binding energy because the question with respect to which QP transition energy cannot be answered.

In the experimental work[29] it was claimed that an additional excitonic feature shifted by about 0.8 eV towards higher energies has been observed. This feature has been interpreted as the $n=2$ exciton peak of a hydrogenlike series with an exciton binding energy of almost 1.1 eV, though the Wannier-Mott-like exciton picture should be inappropriate. The calculated spectrum in Fig. 6 also shows a shoulder at photon energies of about 1 eV higher in energy. However, we cannot really derive the main character (either due to Coulomb effects or due to interband transitions) of this feature. The pronounced exciton peak, the second peak roughly 3.4 eV above the first one, and the absolute values of the spectral strength agree well with the corresponding features in experimental spectra, at least in that measured at room temperature. The low-temperature spectrum exhibits a stronger exciton peak which may be simulated by a smaller broadening parameter.

However, there is a discrepancy between the measured[29] and the calculated (Fig. 6) exciton peak. In the measured spectra this peak is redshifted by about 1 eV. In order to bridge this discrepancy, we include effects of the lattice polarizability in the many-body calculations, at least on the quasiparticle level. We have also performed test calculations (not presented here) with the inclusion of the lattice polarizability in the electron-hole attraction. This leads to a considerable reduction of the excitonic effects and, hence, to a change of the lineshape. In particular, the bound excitonic peak is dramatically reduced. For that reason, we conclude that the dynamics of exciton formation does not allow a substantial contribution of the lattice polarizability to the electron-hole screening and, hence, omit this contribution. Within the Wannier-Mott picture and a reduced pair mass of $0.44\ m$[29] an exciton binding energy of about 1.1 eV would result. This value is indeed large compared with the optical phonon energy of about $\hbar\omega_{LO}=0.03$ eV. Therefore, the lattice polarizability is only taken into account in the QP shifts. In order to account for the vertex corrections we reduce the effect of the lattice polarizability. Numerically we replace ε_0 by the average 3.9 of ε_0 and ε_∞. This procedure leads to a QP gap of about 7.7 eV (cf. Table IV). The resulting imaginary part of the dielectric function is presented in Fig. 7 and compared with the experimental room-temperature spectrum.[29] It seems that this procedure may roughly explain the measured lineshape of the absorption and the measured peak positions. There remain differences. After partial inclusion of the lattice polarizability the high-energy peaks are seemingly too much redshifted and the broad structures around 9.5 or 10.5 eV between the two peaks in the computed spectra are too pronounced. Probably the vertex polaron corrections are stronger for the high-energy transitions compared with the 50% reduction assumed here.

A similar tendency has been observed for the energy loss function $-\mathrm{Im}[1/\varepsilon(\omega)]$ of *rs*-NaCl in Fig. 8. The comparison of the calculated spectrum with the function constructed from measured optical data[29] shows qualitative agreement. All the observed peaks occur in the computed spectrum. However, the majority of the high-energy peaks is too much redshifted and the intensity of the calculated loss spectrum is somewhat to small.

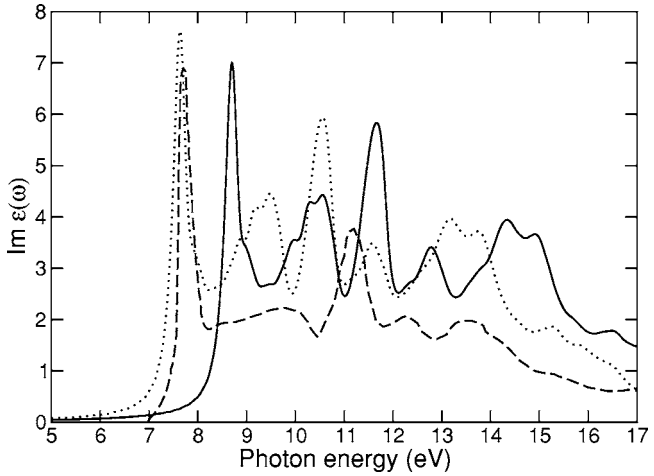

FIG. 7. Imaginary parts of the macroscopic dielectric function calculated including quasiparticle and excitonic effects without (solid line) and with (dotted line) the effect of the lattice polarization for *rs*-NaCl. The experimental room-temperature spectrum (Ref. 29) is shown as dashed line. A Lorentzian broadening of 0.2 eV has been used.

V. SUMMARY

Using a combination of an *ab initio* density functional theory for the ground-state properties and the many-body perturbation theory to describe electronic properties we have studied the band structures and optical spectra of the wide-gap semiconductor AlN and the insulator NaCl. Because of their high static ionicity of the chemical bonds, these crystals also possess large dynamical ion charges $\sim(1/\varepsilon_\infty-1/\varepsilon_0)^{1/2}$ and, hence, a large polarizability of the vibrating lattice. Consequently, in addition to the screening reaction of the inhomogeneous electron gas one also expects a response of the ion lattice after excitation of electrons, holes or electron hole pairs.

In order to simulate the lattice influence we have added the dynamic lattice polarizability to the electronic effect. In

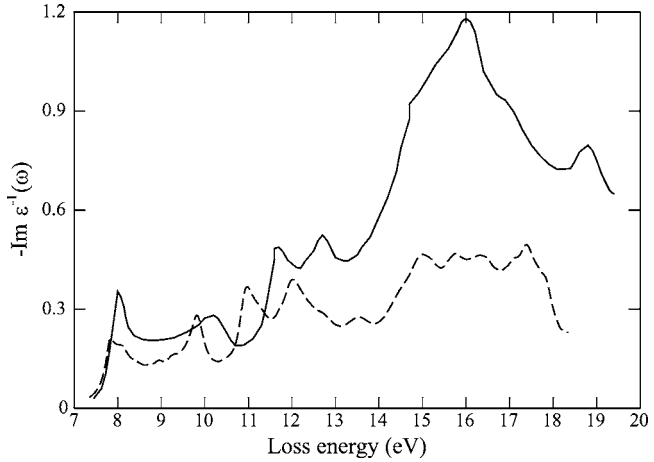

FIG. 8. The energy-loss function for *rs*-NaCl. Solid line: derived from a dispersion analysis of the optical-reflectance data (Ref. 29); dashed line: computed with reduced lattice polaron effects in the QP calculations.

the limit of small frequencies, $\hbar\omega \ll$ gap energy, this approach yields the well-known lattice-polaron effect on single bands in the self-energy of electrons and holes. In the limit of small wave vectors, $q < q_{TF}$, (which is fulfilled for extended effective-mass states) and small frequencies, $\omega < \omega_{TO}$, the Coulomb attraction of electrons and holes can be replaced by the static dielectric constant of the ionic crystal including the lattice polarizability. The opposite limit of pure frequency- and wave-vector-dependent electronic screening is also included.

In the case of quasiparticle bands and gaps we found hints for a reduced lattice polaron effect for AlN. We have discussed this finding in terms of vertex corrections. In the NaCl case the situation is less clear. Comparing the results of the quasiparticle approach only with band positions derived from initial- and final-state photoemission spectroscopy (PES), it seems that the lattice effect can be widely neglected. However, looking for the correct peak positions in optical absorption spectra, a contribution of the lattice polarizability to the quasiparticle shifts seems to be necessary. To bring the bound exciton peak at the absorption onset in agreement with the experimental position a large polaron shift of about 1 eV is needed. For higher optical transitions this shift can be smaller because of the more efficient vertex corrections due to the electron-phonon interaction.

The discussion of the lattice contribution to the screened Coulomb attraction is difficult because it requires studies of the dynamical screening, which, however, does not lead to a closed Bethe-Salpeter equation. For that reason we studied only limiting cases. The nonexistence of Wannier-Mott-like excitons in particular in NaCl makes the conclusions more difficult. However, the large redshifts of the optical absorption with respect to the independent-quasiparticle approach and the complete change of the lineshape in the NaCl case indicate strong excitonic effects, which would mean large exciton binding energies in the Wannier-Mott limit. For that reason, we concluded that the lattice cannot follow the large effects of the Coulomb attraction and, therefore, not contribute to its screening.

ACKNOWLEDGMENTS

This work has been supported by the Deutsche Forschungsgemeinschaft (Project No. Be 1346/18-1) and the European Community in the framework of the Network of Excellence NANOQUANTA (Contract No. NMP4-CT-2004-500198).

*Present address: Universität Paderborn, Fakultät für Naturwissenschaften, Theoretische Physik, Warburger Str. 100, 33100 Paderborn, Germany.

[1] G. Onida, L. Reining, and A. Rubio, Rev. Mod. Phys. **74**, 601 (2002).
[2] I. Vasiliev, S. Ögüt, and J. R. Chelikowsky, Phys. Rev. B **65**, 115416 (2002).
[3] L. Hedin, Phys. Rev. **139**, A796 (1965).
[4] L. Hedin and S. Lundqvist, Solid State Phys. **23**, 1 (1969).
[5] L. J. Sham and T. M. Rice, Phys. Rev. **144**, 708 (1966).
[6] W. Hanke and L. J. Sham, Phys. Rev. Lett. **43**, 387 (1979); Phys. Rev. B **21**, 4656 (1980).
[7] G. Strinati, Phys. Rev. Lett. **49**, 1519 (1982); Riv. Nuovo Cimento **11**, 1 (1988).
[8] P. Hohenberg and W. Kohn, Phys. Rev. **136**, B864 (1964).
[9] W. Kohn and L. J. Sham, Phys. Rev. **140**, A1133 (1965).
[10] M. S. Hybertsen and S. G. Louie, Phys. Rev. B **32**, 7005 (1985).
[11] R. W. Godby, M. Schlüter, and L. J. Sham, Phys. Rev. B **35**, 4170 (1987).
[12] F. Bechstedt, Adv. Solid State Phys. **32**, 161 (1992).
[13] F. Aryasetiawan and O. Gunnarsson, Rep. Prog. Phys. **61**, 237 (1998).
[14] W. G. Aulbur, L. Jönsson, and J. W. Wilkins, Solid State Phys. **54**, 1 (1999).
[15] S. Albrecht, L. Reining, R. Del Sole, and G. Onida, Phys. Rev. Lett. **80**, 4510 (1998).
[16] L. X. Benedict, E. L. Shirley and R. B. Bohn, Phys. Rev. B **57**, R9385 (1998).
[17] M. Rohlfing and S. G. Louie, Phys. Rev. Lett. **81**, 2312 (1998).
[18] M. Rohlfing and S. G. Louie, Phys. Rev. Lett. **83**, 856 (1999).
[19] P. H. Hahn, W. G. Schmidt, and F. Bechstedt, Phys. Rev. Lett. **88**, 016402 (2002).
[20] M. Rohlfing and S. G. Louie, Phys. Rev. Lett. **80**, 3320 (1998).
[21] P. H. Hahn, W. G. Schmidt, K. Seino, M. Preuss, F. Bechstedt, and J. Bernholc, Phys. Rev. Lett. **94**, 037404 (2005).
[22] R. Leitsmann, W. G. Schmidt, P. H. Hahn, and F. Bechstedt, Phys. Rev. B **71**, 195209 (2005).
[23] L. X. Benedict, E. L. Shirley, and R. B. Bohn, Phys. Rev. Lett. **80**, 4514 (1998).
[24] N.-P. Wang, M. Rohlfing, P. Krüger, and J. Pollmann, Phys. Rev. B **67**, 115111 (2003).
[25] L. X. Benedict, T. Wethkamp, K. Wilmers, C. Cobet, N. Esser, E. L. Shirley, W. Richter, and M. Cardona, Solid State Commun. **112**, 129 (1999).
[26] A. Garcia and M. L. Cohen, Phys. Rev. B **47**, 4215 (1993).
[27] M. Born and K. Huang, *Dynamical Theory of Crystal Lattices* (Oxford University Press, Oxford, 1954).
[28] G. D. Mahan, *Many-Particle Physics* (Plenum Press, New York, 1990).
[29] D. M. Roessler and W. C. Walker, Phys. Rev. **166**, 599 (1968).
[30] G. Kresse and J. Furthmüller, Phys. Rev. B **54**, 11169 (1996); Comput. Mater. Sci. **6**, 15 (1996).
[31] J. P. Perdew and A. Zunger, Phys. Rev. B **23**, 5048 (1981).
[32] G. Kresse and D. Joubert, Phys. Rev. B **59**, 1758 (1999).
[33] J. Furthmüller, P. Käckell, F. Bechstedt, and G. Kresse, Phys. Rev. B **61**, 4576 (2000).
[34] E. L. Briggs, D. J. Sullivan, and J. Bernholc, Phys. Rev. B **54**, 14362 (1996).
[35] D. R. Hamann, Phys. Rev. B **40**, 2980 (1989).
[36] S. G. Louie, S. Froyen, and M. L. Cohen, Phys. Rev. B **26**, 1738 (1982).
[37] H. Schulz and K. H. Thiemann, Solid State Commun. **23**, 815

(1977).
[38] F. Bechstedt, in *Low-Dimensional Nitride Semiconductors*, edited by B. Gil (Oxford University Press, Oxford, 2002), p. 11.
[39] I. Petrov, E. Mojab, R. C. Powell, and J. E. Greene, Appl. Phys. Lett. **60**, 2491 (1992).
[40] M. P. Tosi, Solid State Phys. **16**, 1 (1964).
[41] F. Bechstedt, R. Del Sole, G. Cappellini, and L. Reining, Solid State Commun. **84**, 765 (1992).
[42] M. S. Hybertsen and S. G. Louie, Phys. Rev. B **37**, 2733 (1988).
[43] G. Cappellini, R. Del Sole, L. Reining, and F. Bechstedt, Phys. Rev. B **47**, 9892 (1993).
[44] X. Zhu and S. G. Louie, Phys. Rev. B **43**, 14142 (1991).
[45] W. G. Schmidt, J. L. Fattebert, J. Bernholc, and F. Bechstedt, Surf. Rev. Lett. **6**, 1159 (1999).
[46] J. Furthmüller, G. Cappellini, H.-C. Weissker, and F. Bechstedt, Phys. Rev. B **66**, 045110 (2002).
[47] M. Palummo, R. Del Sole, L. Reining, F. Bechstedt, and G. Cappellini, Solid State Commun. **95**, 393 (1995).
[48] B. Wenzien, P. Käckell, F. Bechstedt, and G. Cappellini, Phys. Rev. B **52**, 10897 (1995).
[49] G. Cappellini, V. Fiorentini, K. Tenelsen, and F. Bechstedt, Mater. Res. Soc. Symp. Proc. **395**, 429 (1996).
[50] W. G. Schmidt, S. Glutsch, P. H. Hahn, and F. Bechstedt, Phys. Rev. B **67**, 085307 (2003).
[51] G. Baym and L. P. Kadanoff, Phys. Rev. **124**, 287 (1961).
[52] B. Adolph, J. Furthmüller, and F. Bechstedt, Phys. Rev. B **63**, 125108 (2001).
[53] F. Bechstedt, K. Tenelsen, B. Adolph, and R. Del Sole, Phys. Rev. Lett. **78**, 1528 (1997).
[54] H. J. Monkhorst and J. D. Pack, Phys. Rev. B **13**, 5188 (1976).
[55] P. H. Hahn, K. Seino, W. G. Schmidt, J. Furthmüller, and F. Bechstedt, Phys. Status Solidi B **242**, 2720 (2005).
[56] W. Cochran and R. H. Cowley, J. Phys. Chem. Solids **23**, 447 (1962).
[57] J.-M. Wagner and F. Bechstedt, Phys. Rev. B **66**, 115202 (2002).
[58] H. F. MacDonald, M. V. Klein, and T. P. Martin, Phys. Rev. **177**, 1292 (1969).
[59] K. Shindo, J. Phys. Soc. Jpn. **29**, 287 (1970).
[60] R. Zimmermann, Phys. Status Solidi B **48**, 603 (1971).
[61] F. Bechstedt, R. Enderlein, and M. Koch, Phys. Status Solidi B **99**, 61 (1980).
[62] A. Rubio, J. L. Corkill, M. L. Cohen, E. L. Shirley, and S. G. Louie, Phys. Rev. B **48**, 11810 (1993).
[63] J. Li, K. B. Nam, M. L. Nakami, J. Y. Lin, H. X. Jiang, P. Carrier, and S.-H. Wei, Appl. Phys. Lett. **83**, 5163 (2003).
[64] J. Chen, W. Z. Shen, H. Ogawa, and Q. X. Guo, Appl. Phys. Lett. **84**, 4866 (2004).
[65] M. P. Thompson, G. W. Auner, T. S. Zheleva, K. A. Jones, S. J. Simko, and J. N. Hilfiker, J. Appl. Phys. **89**, 3331 (2001).
[66] Q. Guo and A. Yoshida, Jpn. J. Appl. Phys., Part 1 **33**, 2453 (1994).
[67] I. Vurgaftman and J. R. Meyer, J. Appl. Phys. **94**, 3675 (2003).
[68] C. Stampfl and C. G. Van de Walle, Phys. Rev. B **59**, 5521 (1999).
[69] J. P. Perdew, J. A. Chevary, S. H. Vosko, K. A. Jackson, M. R. Pederson, D. J. Singh, and C. Fiolhais, Phys. Rev. B **46**, 6671 (1992).
[70] P. Jonnard, N. Capron, F. Semond, J. Massies, E. Martinez-Guerro, and H. Mariette, Eur. Phys. J. B **42**, 351 (2004).
[71] F.-J. Himpsel and W. Steinmann, Phys. Rev. B **17**, 2537 (1978).
[72] R. T. Poole, J. G. Jenkin, J. Liesegang, and R. C. G. Leckey, Phys. Rev. B **11**, 5179 (1975).
[73] R. Haensel, G. Keitel, G. Peters, P. Schreiber, B. Sonntag, and C. Kunz, Phys. Rev. Lett. **23**, 530 (1969).
[74] T. Timusk and W. Martienssen, Phys. Rev. **128**, 1656 (1962).
[75] A. E. Carlsson, Phys. Rev. B **31**, 5178 (1985).
[76] W. A. Harrison, *Elementary Electronic Structure* (World Scientific, Singapore, 1999).
[77] P. K. de Boer and R. A. de Groot, Am. J. Phys. **67**, 443 (1999).
[78] S. T. Pantelides, Phys. Rev. B **11**, 2391 (1975); **11**, 5082 (1975).
[79] V. Cimalla, V. Lebedev, U. Kaiser, R. Goldhahn, Ch. Foerster, J. Pezoldt, and O. Ambacher, Phys. Status Solidi C **2**, 2199 (2005).
[80] B. E. Foutz, S. K. O'Leary, M. S. Shur, and L. F. Eastman, J. Appl. Phys. **85**, 7727 (1999).
[81] T. Wethkamp, K. Wilmers, C. Cobet, N. Esser, W. Richter, O. Ambacher, M. Stutzmann, and M. Cardona, Phys. Rev. B **59**, 1845 (1999).